Ocean Dynamics (2014) 64:429–441
DOI 10.1007/s10236-014-0692-y

Multimodal particle size distributions of fine-grained sediments: mathematical modeling and field investigation

Byung Joon Lee · Erik Toorman · Michael Fettweis

Received: 21 January 2013 / Accepted: 16 January 2014 / Published online: 1 February 2014

Abstract Multimodal particle size distributions (PSDs) of fine-grained cohesive sediments are common in marine and coastal environments. The curve-fitting software in this study decomposed such multimodal PSDs into subordinate log-normal PSDs. Four modal peaks, consisting of four-level ordered structures of primary particles, flocculi, microflocs, and macroflocs, were identified and found to alternately rise and sink in a flow-varying tidal cycle due to shear-dependent flocculation. The four modal PSD could be simplified further into two discrete size groups of flocculi and flocs. This allowed the development of a two-class population balance equation (TCPBE) model with flocculi and flocs to simulate flocculation involving multimodal PSDs. The one-dimensional vertical (1-DV) TCPBE model further incorporated the Navier-Stokes equation with the k-ε turbulence closure and the sediment mass balance equations. Multimodal flocculation as well as turbulent flow and sediment transport in a flow-varying tidal cycle could be simulated well using the proposed model. The 1-DV TCPBE was concluded to be the simplest model that is capable of simulating multimodal flocculation in the turbulent flow field of marine and coastal zones.

Keywords Cohesive sediments · Flocculation · Multimodal · Particle size distribution · Population balance equations

Responsible Editor: Han Winterwerp

This article is part of the Topical Collection on the *11th International Conference on Cohesive Sediment Transport*

B. J. Lee (✉)
School of Constructional and Environmental Engineering, Kyungpook National University, 2559 Gyeongsang-daero, Sangju, Gyeongbuk 742-711, South Korea
e-mail: bjlee@knu.ac.kr

E. Toorman
Hydraulics Laboratory, Department of Civil Engineering, KU Leuven, Kasteelpark Arenberg 40, 3001 Leuven, Belgium

M. Fettweis
OD Natural Environment, Royal Belgian Institute of Natural Sciences, Gulledelle 100, 1200 Brussels, Belgium

1 Introduction

Fine-grained cohesive sediments undergo a range of physical, chemical, and biological processes while traveling from an upstream river to a downstream estuary or coast. The physical processes include advection, dispersion, sedimentation, flocculation, etc. The chemical processes include chemical reactions occurring in solution and on the sediment surface, and biological processes involve a range of activities of microorganisms, plants, and animals. Among the many physical, chemical, and biological processes, flocculation has been reported to be the most important process for determining the size, settling velocity, and deposition rate of fine-grained cohesive sediment particles in a marine and coastal environment (e.g., Krone 1962; Gibbs 1985; Fettweis 2008; Manning et al. 2006).

Flocculation is the combined process of particle size growth and decay by aggregation and breakage in a turbulent flow field, and can determine the size and settling velocity of the cohesive sediment particles (van Leussen 1994; Winterwerp and van Kesteren 2004). Low turbulent flow enhances particle aggregation and increases the size and settling velocity of cohesive sediment particles, but high turbulent flow enhances floc breakage and decreases the size and settling velocity. Moreover, flocculation in the marine and coastal environment develops a multimodal particle size distribution (PSD) with four-level ordered aggregate structures of primary particles, flocculi (a compound word of floc and nuclei), microflocs, and macroflocs (Fig. 1) (Michaels and

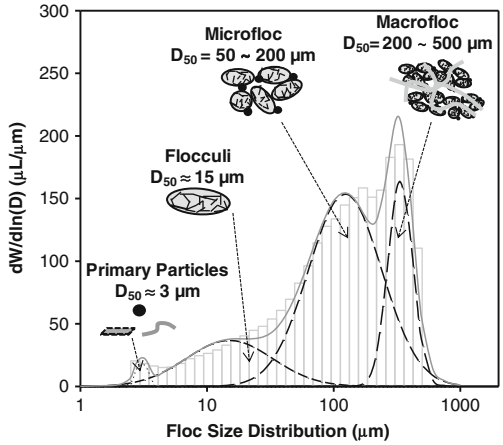

Fig. 1 Multimodal PSD and schematic diagrams of the four-level ordered aggregate structures of primary particles, flocculi, microflocs and macroflocs, modified from Lee et al. (2011)

Bolger 1962; Firth and Hunter 1976; Francois 1985; van Leussen 1994). Multimodal particle size distributions have been reported to determine the fate of sediments by controlling settling (e.g., Fettweis et al. 2012; Lee et al. 2012) and erosion/deposition (e.g., Letter and Mehta 2011).

Many mathematical models have been developed to simulate the flocculation of cohesive sediments in marine and coastal environments. Some flocculation models are realistic with substantial computations, whereas others are approximate with relatively small computations. For example, a multi-class population balance equation (PBE) is realistic for simulating the flocculation of many particles and floc size groups but it is mathematically complicated with many coupled differential equations (e.g., Verney et al. 2011; Xu et al. 2008). A single-class PBE is mathematically simple and robust with only one floc size group but is unable to simulate flocculation involving multimodal PSDs, which is referred to as multimodal flocculation. Therefore, a two-class PBE (TCPBE) consisting of the discrete size groups of flocculi and flocs was developed recently to simulate multimodal flocculation, particularly bimodal flocculation, with a minimum number of equations and computations (Lee et al. 2011, 2012). Sophisticated flocculation models with many discrete floc size classes (e.g., Verney et al. 2011; Xu et al. 2008) or a continuous size distribution (e.g., Maerz and Wirtz 2009) would be more accurate and precise than the TCPBE for simulating multimodal flocculation. On the other hand, the TCPBE can be a practical alternative to such sophisticated models with less computational cost, considering that a combination of two discrete size groups of flocculi and flocs can approximate a multimodal PSD. The TCPBE is at least better for simulating multimodal flocculation than many contemporary flocculation models with a single floc size group (e.g., Son and Hsu 2009; Winterwerp 1998).

To simulate the fate of fine-grained cohesive sediments in a marine and coastal environment correctly, a flocculation model must be solved in a coupled manner with hydrodynamic and sediment transport models. For example, hydrodynamics controls the flocculation kinetics for determining the floc size growth and decay rates by shear-dependent flocculation in a turbulent flow field. The flocculation kinetics then controls sediment transport because it determines the size, settling velocity, and deposition rate of cohesive sediment particles. Hydrodynamics also controls the sediment transport for determining the advection and dispersion of cohesive sediment particles. Sediment transport gives a feedback to hydrodynamics, such as a turbulence reduction due to stratification of the sediment concentration.

In this study, a one-dimensional vertical (1-DV) TCPBE, combining the Reynolds-averaged Navier-Stokes (RANS) equation with the k-ε turbulence closure, sediment mass balance equation, and TCPBE, was developed to simulate the interactive processes shown above. The RANS equation with the k-ε turbulence closure, sediment mass balance equation and TCPBE were used to simulate turbulent flow, sediment transport, and the flocculation kinetics, respectively. This paper reports the behavior of multimodal PSDs of fine-grained cohesive sediments in a flow-varying tidal cycle and validates the capability of the 1-DV TCPBE for simulating multimodal flocculation and cohesive sediment transport.

2 Mathematical models

2.1 Fluid mechanics and sediment transport equations

The RANS equations were used to simulate flow movement. For a one-dimensional vertical water column, the RANS equations were simplified to a streamwise momentum conservation equation, neglecting advection, as shown in Eq. (1). The equation incorporated the eddy viscosity but discarded the molecular viscosity because (far enough from the bed) the former is several orders higher than the latter in a marine and coastal zone.

$$\frac{\partial U}{\partial t} = \frac{\partial}{\partial z}\left(C_\mu \frac{k^2}{\varepsilon}\frac{\partial U}{\partial z}\right) - \frac{1}{\rho}\frac{\partial p}{\partial x} \tag{1}$$

In Eq. (1), U is the time averaged velocity component, t and z are time and space, ρ is the fluid density, p is the piezometric pressure, C_μ is an empirical scaling parameter, k is the turbulent kinetic energy, and ε is the turbulent energy dissipation rate. Assuming local equilibrium of the flow field, the horizontal pressure gradient term (the last term of Eq. (1)) is approximated by U_*^2/H, where U_* and H are the measured friction velocity and water height, respectively. Only the friction velocity (U_*) and water height (H)

were available for calculating the horizontal pressure gradient term (see Section 3.1).

The sediment mass balance equation was used to simulate the one-dimensional vertical transport of flocculi and flocs in the water column (Eq. (2)). As shown in Fig. 2, size-fixed flocculi and size-varying flocs approximate a bimodal PSD varying in time and space. To track the three time- and space-dependent variables, the number concentration of flocculi (N_P) and the size and number concentration of flocs (D_F and N_F), the sediment mass balance equation incorporates three differential equations for the time rate of change in the following: (1) the number concentration of flocculi in suspension (dN_P/dt), (2) the number concentration of flocs in suspension (dN_F/dt), and 3) the number concentration of flocculi bound in flocs (dN_{PF}/dt). On the right-hand side of Eq. (2), the respective terms represent turbulence-mediated dispersion, gravity-driven sedimentation, and flocculation kinetics. The flocculation kinetics (A_i+B_i) incorporates the TCPBE, which can simulate bimodal flocculation (see also Section 2.3).

$$\frac{\partial N_i}{\partial t} = \frac{\partial}{\partial z}\left(C'_{\mu}\frac{k^2}{\varepsilon}\frac{\partial N_i}{\partial z}\right) - w_{s,i}\frac{\partial N_i}{\partial z} + (A_i + B_i) \tag{2}$$

In Eq. (2), $N_i = N_i(z, t)$ represents the number concentration, subscript i represents flocculi and flocs in suspension (N_P and N_F) and the flocculi bound in flocs ($N_{PF} = N_C \times N_F$), N_C is the floc size index representing the number of flocculi bound in a floc, C'_{μ} is an empirical scaling parameter (A_i+B_i) is the respective growth and decay rates of N_i by aggregation and breakage, and $w_{s,i}$ is the settling velocity of flocculi or flocs.

The modified Stokes equation, including the use of fractal theory for floc packing and shaping, and the Schiller's equation for the turbulent drag correction, was used to calculate the floc settling velocity ($w_{s,i}$) (Schiller 1932). The Richardson-Zaki equation was also included to calculate the correction factor (Φ_{HS}) for hindered settling in a highly concentrated near-bottom mud layer (Eqs. (3) and (4)) (Richardson and Zaki 1954; Winterwerp 1998), even though it was only valid for relatively low concentrations (Toorman 1999).

$$w_{s,i} = \Phi_{HS}\left(\frac{1}{18}\frac{(\rho_s - \rho_w)g}{\mu}D_P^{3-nf}\frac{D_i^{nf-1}}{1 + 0.15\mathrm{Re}_i^{0.687}}\right) \tag{3}$$

$$\Phi_{HS} = (1-\phi)^a \qquad \phi << \phi_{\max} \approx 0.7 \tag{4}$$

In Eqs. (3) and (4), D_p=size (diameter) of flocculi (i.e., the group of primary particles and flocculi), D_i is the size of ith class particles or flocs, D_F is the size of flocs (i.e., the group of microflocs and macroflocs), replacing D_i in Eq. (3), n_f is the fractal dimension for describing the particle-organizing scheme in a floc, ρ_s is the particle density, ρ_w is the fluid density, g is the gravitational acceleration, μ is the fluid viscosity, Φ_{HS} is the correction factor for hindered settling, Φ is the volumetric concentration of flocs (cubic meter flocs per cubic meter), and Re_i is the Reynolds number of a particle or floc ($=D_i \cdot w_{s,i} \cdot \rho_w/\mu$).

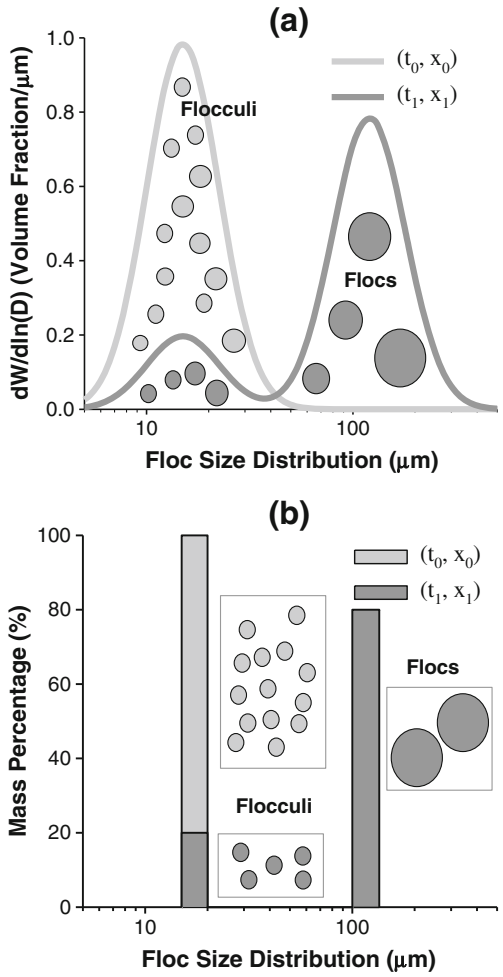

Fig. 2 Schematic diagrams of **a** continuous particle size distributions and **b** discrete size groups of flocculi and flocs before and after flocculation, from (t_0, x_0) to (t_1, x_1). **b** also represents the flocculation strategy of the TCPBE

2.2 Turbulence closure

The two-equation k-ε turbulence closure was selected to simulate the fluid turbulence, which consequently controls the turbulence-mediated sediment dispersion and flocculation (Eqs. (5) and (6)). The two-equation model has the two differential equations for the conservation of turbulent kinetic energy and its dissipation rate (k and ε), and incorporates the

turbulent kinetic energy production and buoyancy destruction terms (P and G). In particular, the buoyancy destruction term (G) is incorporated to simulate the particle-fluid interactions, considering the damping effect of sediment stratification on the fluid turbulence. The buoyancy by stable sediment stratification can destroy or dampen the flow turbulence (Burchard and Baumert 1998; Rodi 1980; Toorman 2003).

$$\frac{\partial k}{\partial t} = \frac{\partial}{\partial z}\left(\frac{C_\mu}{\sigma_k}\frac{k^2}{\varepsilon}\frac{\partial U}{\partial z}\right) + P + G - \varepsilon \tag{5}$$

$$\frac{\partial \varepsilon}{\partial t} = \frac{\partial}{\partial z}\left(\frac{C_\mu}{\sigma_\varepsilon}\frac{k^2}{\varepsilon}\frac{\partial \varepsilon}{\partial z}\right) + C_1\frac{\varepsilon}{k}(P + C_3 G) - C_2\frac{\varepsilon^2}{k} \tag{6}$$

In Eqs. (5) and (6), the standard model coefficients were applied: σ_k=1.0, σ_ε=1.3, C_1=1.44, C_2=1.92 and C_3=−1.4 (Burchard and Baumert 1998; Conley et al. 2008).

The turbulent kinetic energy production term (P) and the buoyancy destruction term (G) are expressed in Eqs. (7) and (8), respectively. The turbulent Schmidt number is closed with the Munk-Anderson damping functions, Eq. (9) (Munk and Anderson 1948). The gradient Richardson number (Ri) is a dimensionless measure of the stability of stratification (Eq. (10)). Under the stratification effect (Ri>0), the damping effect on turbulence will be considered by the buoyancy destruction term (G) and the stability coefficient of the eddy viscosity (C_μ').

$$P = C_\mu\frac{k^2}{\varepsilon}\left(\frac{\partial U}{\partial z}\right)^2 \tag{7}$$

$$G = C_\mu'\frac{k^2}{\varepsilon}\frac{g}{\rho_o}\frac{\partial \rho}{\partial z} \tag{8}$$

$$\begin{aligned} C_\mu' &= C_\mu\frac{(1+10R_i)^{1/2}}{(1+1.33R_i)^{3/2}} \quad \text{for } R_i \geq 0 \\ &= C_\mu = 0.09 \quad \text{for } R_i < 0 \end{aligned} \tag{9}$$

$$R_i = -\left(\frac{g}{\rho_o}\frac{\partial \rho}{\partial z}\right)\Big/\left(\frac{\partial^2 U}{\partial z^2}\right) \tag{10}$$

Table 1 lists the boundary conditions of the time- and space-dependent variables. The top boundary conditions of flow velocity (U) and turbulent kinetic energy and dissipation rate (k and ε) were treated as a closed boundary (i.e., zero-flux boundary), but the bottom boundary conditions incorporated the friction velocity (U_*) describing flow over a rough bottom boundary. The top boundaries of the number concentrations of flocculi in suspension, flocs in suspension and flocculi bound in flocs (N_P, N_F and N_{PF}) were set to be a closed boundary, but the bottom boundaries were open for erosion and deposition, following the formulations of shear-dependent erosion and continuous deposition (Eqs. (11) and (12)) (Ariathurai 1974; Le Hir et al. 2011; Winterwerp 1998). In the 1-DV TCPBE model, both flocculi and flocs were subject to deposition, but only flocculi to erosion, which may be referred to as entrainment or disruption (Winterwerp and van Kesteren 2004).

$$E_P = \frac{M}{(\pi/6)D_P^3\rho_P}(\tau/\tau_c - 1) \quad \text{if} \quad B > 0 \text{ and } \tau > \tau_c \tag{11}$$

$$D_i = w_{s,i}N_i \tag{12}$$

In Eq. (12), subscript i is P, F or PF, representing flocculi in a suspension, flocs in suspension and flocculi bound in flocs, respectively. M is the empirical erosion rate parameter, τ is the bottom shear stress, and τ_c is the critical shear stress for erosion. The denominator over M is used to convert the mass concentration to the number concentration. The erosion of flocculi (E_P) is effective only when a pool of erodible sediments is available on the bottom (B>0) and the bottom shear stress is over the critical shear stress (τ>τ_c), according to the Ariathurai-Partheniades equation (Ariathurai 1974).

2.3 Flocculation Kinetic Model

The two-class PBE includes size-fixed flocculi and size-varying flocs as building blocks and buildings, respectively, to simulate bimodal flocculation (Fig. 2). The number of flocculi bound in a floc (N_C) is used as an index of the floc size in the TCPBE. As this new size index becomes one for flocculi (N_C=1), it gives the simplicity of the TCPBE. The TCPBE incorporates three coupled differential equations describing the time rate of change in: (1) the number concentration of microflocs (dN_P/dt), (2) the number concentration of macroflocs

Table 1 Top and bottom boundary conditions of the Navier-Stokes equation with the k-ε turbulence closure and sediment mass balance equation

Boundary conditions at the bottom	$U_b = \frac{U_*}{\kappa}\ln\frac{z_b}{z_o}$	$k_b = \frac{U_*^2}{\sqrt{C_\mu}}$	$\varepsilon_b = \frac{U_*^3}{\kappa \cdot z_o}$	$\left(w_{s,i}N_i - C_\mu' \frac{k^2}{\varepsilon}\frac{\partial N_i}{\partial z}\right)_{z=z_b} = E_i - D_i$
Boundary conditions at the top	$\left(\frac{\partial U}{\partial z}\right)_{z=z_s} = 0$	$\left(\frac{\partial k}{\partial z}\right)_{z=z_s} = 0$	$\left(\frac{\partial \varepsilon}{\partial z}\right)_{z=z_s} = 0$	$\left(w_{s,i}N_i - C_\mu' \frac{k^2}{\varepsilon}\frac{\partial N_i}{\partial z}\right)_{z=z_s} = 0$

(dN_F/dt), and (3) the total number concentration of microflocs bound in macroflocs (dN_{PF}/dt) ($N_{PF}=N_C\times N_F$) (Eq. (13)), and they were incorporated to the growth and decay rates (A_i+B_i) of Eq. (2). Lee et al. (2011) explained the TCPBE in depth.

$$
\begin{aligned}
(A_P + B_P) &= -\frac{1}{2}\alpha\beta_{PP}N_PN_P\left(\frac{N_C}{N_C-1}\right) - \alpha\beta_{PF}N_PN_F + fN_Ca_FN_F \\
(A_F + B_F) &= +\frac{1}{2}\alpha\beta_{PP}N_PN_P\left(\frac{1}{N_C-1}\right) - \frac{1}{2}\alpha\beta_{FF}N_FN_F + a_FN_F \\
(A_{PF} + B_{PF}) &= +\frac{1}{2}\alpha\beta_{PP}N_PN_P\left(\frac{N_C}{N_C-1}\right) + \alpha\beta_{PF}N_PN_F - fN_Ca_FN_F
\end{aligned}
\tag{13}
$$

In Eq. (13), f is the fraction of flocculi generated by floc breakage. α is the collision efficiency factor, β is the collision frequency factor, and a is the breakage kinetic constant. The collision efficiency factor (α) is generally used as an application-specific fitting parameter, and the collision frequency factor (β) is applied as a theoretical function correlated with Brownian motion, turbulent shear rate, and differential settling. Table 2 lists the aggregation and breakage kernels for the collision frequency factor (β) and the breakage kinetic constant (a) (Burd and Jackson 2002; Lee et al. 2011). The aggregation kernels consist of the theoretical functions of Brownian motion, differential settling and turbulent shear, but the breakage kernel is composed of only the shear-dependent breakage kinetics function.

Table 2 Aggregation and breakage kernels of the 1-DV TCPBE modified from Lee et al. (2011)

Aggregation kernel	Breakage kernel
$\beta_{BR,ij} = \frac{2kT}{3\mu}\left(\frac{1}{D_i}+\frac{1}{D_j}\right)(D_i+D_j)$ $\beta_{SH,ij} = \frac{1}{6}(D_i+D_j)^3 G$ $\beta_{DS,ij} = 2\pi D_i^2\lvert w_{s,i} - w_{s,j}\rvert$	$a_i = E_b G\left(\frac{D_i - D_p}{D_p}\right)^p \left(\frac{\mu G}{F_y/D_i^2}\right)^q$

D_i diameter of a particle size class i, β_{BR} collision frequency factor by Brownian motion, β_{SH} collision frequency factor by fluid shear, β_{DS} Collision frequency factor by differential settling, k Boltzmann's constant, T absolute temperature (K), p, q Empirical parameters, μ Absolute viscosity of the fluid, G fluid turbulent shear rate (per second), w_i sedimentation velocity of size class i, E_b breakage efficiency factor, F_y yield strength of flocs (10^{-10} Pa)

2.4 Numerical methods

The operator splitting algorithm and Gauss-Seidel iteration were applied to solve the nonlinear partial differential equations of the 1-DV TCPBE model (Eqs. (1)–(13)). According to the operator splitting algorithm, the flocculation kinetic equations (Eq. (13)) were decoupled and solved explicitly in each time step, to cope with the complexity and nonlinearity (Aro et al. 1999; Winterwerp et al. 2006). Each operator was solved using the Gauss-Seidel iterative method, in which the dependent variables are updated iteratively until the convergence limit in each time step is satisfied. The converged values were then used as the seeding values of the next time step.

Tide equations (Eqs. (14) and (15)) that fit a time series of the measured friction velocity (U_*) and water height (H) in a flood-ebb tidal cycle were used as the input of the momentum conservation equation for driving turbulent flow.

$$U_* = 0.035 - 0.015\cdot\mathrm{COS}(2\cdot 2\pi/(12.4)\cdot t[\mathrm{h}] + 0.5) \tag{14}$$

$$H = 7.4 - 2.0\cdot\mathrm{COS}(2\cdot 2\pi/(24.8)\cdot t[\mathrm{h}] + 4.0) \tag{15}$$

Note that the water height changes during a tidal cycle. To account for the change in water height, the equally spaced grid cells along the water column were set to change their size with

increasing time. Each transport equation (i.e. Eqs. (1), (2), (5), (6); $X=U, N_i, k, \varepsilon$) was corrected with an additional advection term (Eq. (16)) based on the Arbitrary Euler-Lagrange (ALE) method (Huerta and Liu 1988).

$$\left(\frac{\Delta z(t)-\Delta z(t-\Delta t)}{\Delta t}\right)\frac{\partial X(z,t)}{\partial z} \tag{16}$$

where $z(t)$ is the elevation of a node at time t.

3 Material and methods

3.1 Field Measurements

The study area was located in the Belgian coastal zone facing the southern North Sea. This area is of interest because of the occurrence of a coastal high turbidity area. The measurements indicated variations in the SPM concentration near the shore area of 20–70 mg l^{-1} and reaching 100 to >3,000 mg l^{-1} near the bed (Fettweis et al. 2010). Because substantial mud deposition formed over a broad area near the measuring site, the effect of horizontal advection and dispersion, rather than 1-DV processes, was assumed to be minor. The SPM is characterized by the development of multimodal PSD (Fettweis et al. 2012; Lee et al. 2012). Grain size analysis found that the suspended matter in the study area consisted mostly of clay (41 %) and silt (57 %) with a small amount of sand (2 %) (Fettweis 2008). Therefore, flocculation was supposed to be the major contributor for developing a multimodal PSD of such fine-grained cohesive sediments. Tides are semi-diurnal with a mean tidal range at Zeebrugge of 4.3 m (2.8 m) at the spring (neap) tide and maximum current velocities of more than 1 m s^{-1}. Tidal ellipses are commonly well-aligned with the coastline orientation. A tripod was deployed approximately 1 km from the shore line in a water depth of 5.5 m below MLLWS (mean lowest low water at spring tide), and the current velocity, turbulent shear, salinity and suspended sediment were measured in the field measurement campaign from the 15th of April 2008 to the 30th of April 2008. Sediment samples near the tripod showed variable sediment characteristics (fine sand, silt/clay) with a D_{50} grain size of the sand fraction of approximately 150 μm. The measuring instruments on the tripod were a 5 MHz SonTek^R Acoustic Doppler Velocimeter (ADV Ocean), a 3 MHz SonTek^R Acoustic Doppler Profiler (ADP), two D&A^R optical backscatter sensors (OBS), a Sea-bird^R SBE37 CT system, a Sequoia Scientific^R Laser In Situ Scattering & Transmissometer 100C (LISST-100C), and two SonTek^R Hydra systems for data storage and batteries. The values measured from OBS, LISST, and ADV were averaged over each 10-min period and recorded. Two OBSs measured the SPM concentrations at 0.2 and 2 m above the bed (mab). The ADV measured a time series of flow velocity and turbulent intensity at 0.2 mab. The respective horizontal x and y velocity components (U and V) were projected to the alongshore axis directed to the northeast (65°) and the cross-shore axis directed to the southeast (155°) (Baeye et al. 2011). The high frequency ADV (25 Hz) measurements allowed the velocity to be decomposed in terms of a mean and fluctuating part and to calculate the turbulent kinetic energy (TKE) and bottom friction velocity (U_*) with the inertial dissipation method (Fettweis et al. 2010; Sherwood et al. 2006; Trowbridge and Elgar 2001). The LISST-100C, which was attached to the tripod at 2 mab measured the size distribution of the volume-equivalent spherical particle/flocs in 32 logarithmically spaced size groups over the range of 2.5–500 μm (Agrawal and Pottsmith 2000).

3.2 Decomposition of a Multimodal PSD

The observed multimodal (four-peaked) PSD was assumed to be formed by four overlapping unimodal log-normal PSDs of the primary particles, flocculi, microflocs, and macroflocs (Fig. 1). The data was used as the input to the selected software (DistFit^{TM}; Chimera Technologies, USA) which performed curve-fitting analysis and the decomposition of the observed PSD into the subordinate log-normal PSDs (Eq. (17)) (Lee et al. 2012; Whitby 1978).

$$\frac{\mathrm{d}V}{\mathrm{d}D}=\sum_{i=1}^{4}\frac{\overline{V_i}}{\sqrt{2\pi}\ln(\sigma_i)}\exp\left[-\frac{1}{2}\left(\frac{\ln\left(D/\overline{D_i}\right)}{\ln(\sigma_i)}\right)^2\right] \tag{17}$$

In Eq. (17), V and D are the volumetric concentration and diameter of each size interval of the LISST-100C measured PSD, respectively. $\mathrm{d}V/\mathrm{d}D$ is the normalized volumetric fraction by the width of the size interval and is used for curve-fitting to a log-normal distribution (Hinds 1999). $\overline{D_i}$ is the geometric mean diameter $\left(\overline{D}_{g,i}\right)$, which is equivalent to the median diameter ($D_{50,i}$) for a log-normal distribution (Weisstein 2006), σ_i is the geometrical standard deviation, and $\overline{V_i}$ is the volumetric concentration of an ith unimodal PSD. Eq. (17) has twelve fitting parameters for $\overline{D_i}$, σ_i and $\overline{V_i}$ of primary particles, flocculi, microflocs, and macroflocs. Based on the observation, the mean diameters of the primary particles, flocculi, microflocs, and macroflocs were limited to 3, 15, 20~200 and 200~500 μm, respectively, in curve-fitting analysis. The best-quality PSD provided parameter values ($\overline{D_i}$, σ_i and $\overline{V_i}$) for the subordinate log-normal PSDs of the primary particles, flocculi, microflocs, and macroflocs. The resulting parameter values were then used as indicators of cohesive sediment flocculation and transport dynamics. The

smaller and larger two fractions of the decomposed four-class distribution (i.e., primary particles+flocculi and microflocs+macroflocs) were summed up further to a two-class distribution (i.e., flocculi and flocs), and the two volume-weighted mean diameters were calculated for the smaller and larger fractions. The volume fractions and volume-weighted mean diameters were then used for model calibration and validation of 1-DV TCPBE.

3.3 Model calibration and validation

The best-quality simulation of the 1-DV TCPBE, which was fitted to the experimental data, was obtained while changing the adjustable fitting parameters of the collision and breakage efficiency factors (α and E_b), erosion constants (M and τ_c) and floc characteristics (ρ_p and n_f). On the other hand, the other kinetic and physicochemical constants and the initial conditions were fixed at the standard values, which have been found in previous studies (Table 3) (Burchard and Baumert 1998; Lee et al. 2011; Luyten et al. 2002; Winterwerp and van Kesteren 2004). The simulated results of the 1-DV TCPBE were compared with the experimental data from field measurements.

4 Results and discussion

4.1 Field observation on multimodal PSDs

The flood and ebb tidal flows were almost symmetrical during the entire measuring period and were characterized by the similar magnitude of the flow velocities but with opposite alongshore directions. The median floc size (D_{50}) and particle size distribution (PSD) of the cohesive sediments varied as a function of the flood-ebb tidal flows (Fig. 3). During the slack water, the D_{50} reached a maximum and the PSDs were skewed towards the larger size classes with a substantial amount of microflocs and macroflocs (e.g., t=7.00 and 14.50 hours). During peak flow, the D_{50} was minimal and the PSDs were skewed towards the smaller sized classes with a substantial number of primary particles and flocculi (e.g., t=4.33 and 10.17 hours).

Flocculation is controlled mainly by fluid turbulent shear that determines the D_{50} and PSDs during a tidal cycle (Fettweis et al. 2006). Low turbulence during slack water enhances aggregation and reduces breakage, whereas the opposite occurs during peak flow conditions. This behavior agrees well with the findings of the present study, and points to the occurrence of mainly fine-grained cohesive sediments in suspension at the measuring site (e.g., clay and silt) (see Section 3.1), rather than sand particles. The latter would not affect D_{50} or PSDs in the observed way.

The height of the four modal peaks of the primary particles, flocculi, microflocs, and macroflocs changed as a function of the turbulence intensity during the tide, resulting in different multimodal PSDs (Fig. 3c). During the peak flow condition, the peaks of the primary particles and flocculi (the first and second peaks from the left of a PSD) increased, whereas the peaks of micro- and macroflocs (the third and fourth peaks) (e.g., 4.33 and 10.17 hours) decreased. The opposite was observed during slack water (e.g., 7.00 and 14.50 hours). For many PSDs, peaks recurred at approximately 3 and 15 μm with small variations, which were defined as the modal peaks of the primary particles and flocculi, respectively. The other peaks were defined as the modal peaks of microflocs and macroflocs, and recurred at 50~200 and 200~500 μm, respectively, with large variations in the floc size caused by aggregation and breakage (see also Fig. 1). These four-level ordered aggregate structures of primary particles, flocculi, microflocs, and macroflocs are common in marine and coastal environments (Lee et al. 2012; van Leussen 1994). The primary particles are fine particles consisting of fragmented clay particles, organic and calcareous particles, picophytoplankton and bacteria. The primary particles are often smaller than the size range of the LISST 100C; these fine "out of range" particles affect the entire PSD, with a significant increase in the volume concentration of the smallest two size classes (Andrews et al. 2010) explaining the rising tail in Fig. 3c during peak flow (e.g., 4.33 and 10.17 hours). Flocculi, which are seldom broken down to the lowest-level primary particles, are considered the major building blocks of flocs rather than primary particles in a marine and coastal environment. Microflocs and macroflocs form with flocculi and primary particles because of the physicochemically and biologically mediated flocculation in the salt- and biomass-enriched sea water (Eisma 1986; van Leussen 1994).

4.2 Numerical Simulation of Multimodal Flocculation

The four-level ordered aggregate structures of the primary particles, flocculi, microflocs and macroflocs may be simplified further to a two-level structure of flocculi (primary particles and flocculi) and flocs (microflocs and macroflocs) for modeling and simulation (Lee et al. 2012). The sharp peak of the primary particles, which in reality consists mostly of out-of-range particles below the lowest measurable size, can merge to the peak of flocculi. Furthermore, settling flux analysis of the multimodal PSDs showed the two discrete size groups of flocculi and flocs could approximate a continuous multimodal PSD with a relatively small error less than 9.5 % (Lee et al. 2012). Therefore, the TCPBE with size-fixed flocculi and size-varying flocs has been proposed as the simplest model that is capable of simulating multimodal flocculation (see also Fig. 2b) (Lee et al. 2011).

Table 3 Parameters and initial conditions of the 1-DV TCPBE for the best-quality simulation

Kinetic parameters and physicochemical constants			
Classification	Symbol	Value	Description
Flocculation kinetics	α	0.2	Collision efficiency factor [−]
	E_b	3.0e-5	Efficiency factor for breakage [$s^{0.5}$/m]
	F_y	1.0e-10	Yield strength of flocs [Pa]
	f	1.0	Fraction of flocculi by breakage [−]
	p[a]	1.0	Empirical parameter of breakage kinetics
	q	3.0 - n_f	Empirical parameter of breakage kinetics
Turbulent flow	C_μ	0.09	Model fitting coefficients [−]
	C_1	1.44	
	C_2	1.92	
	C_3	−1.4	
	σ_k	1.0	
	σ_ε	1.3	
	κ	0.4	Von Karmen's coefficient [−]
	z_o	0.001	Bottom roughness length [m]
	z_b	0.01	Distance from the bottom [m]
Erosion deposition	M	1.0e-3	Empirical erosion parameter [$kg/m^2/s$]
	t_c	1.5	Critical shear stress for erosion [pa]
	B	2.24	Total mass of erodible sediments [kg/m^2]
Sediment property	ρ_P	1800	Density of flocculi [kg/m^3]
	ρ_w	1050	Density of sea water [kg/m^3]
	D_P	15.0	Diameter of flocculi [μm]
	n_f	2.3	Fractal dimension of flocs [−]
	a	4.0	Exponent of Richardson-Zaki eqn [Pa]
Initial conditions (at t=0)			
Sediment concentration	c	0.32	Total mass conc. of sediments [g/L]
	N_{PT}[b]	1.004e+11	No. conc. of flocculi [$/m^3$]
Seeding flocs	D_{F0}	100	Diameter of seeded flocs [μm]
	$Frac_{F0}$	0.1	Mass fraction of seeded flocs [−]
TCPBE	N_{P0}	$(1-\mathrm{Frac}_{F,0})\ N_{PT}$	No. conc. of flocculi [$/m^3$]
	N_{F0}	$(D_{F,0}/D_P)^{-nf}\ (\mathrm{Frac}_{F,0})\ N_{PT}$	No. conc. of flocs [$/m^3$]
	N_{PF0}	$(Frac_{F,0})\ N_{PT}$	No. conc. of flocculi bound in Flocs [$/m^3$]

[a] p was set as 1.0 to narrow FSDs, instead of 0.5 of Winterwerp and van Kasteren (2004)

[b] $N_{PT}=c/(0.167\cdot\pi\cdot D_P{}^3)/\rho_S$, assuming that flocculi are spherical

The collision and breakage efficiency factors (α and E_b), erosion constants (M and τ_c) and floc characteristics (ρ_p and n_f) were selected as the adjustable fitting parameters to identify the best-quality simulation. The collision efficiency factor (α) of the best-quality simulation was 0.2 within the theoretical range between 0 and 1, and the breakage efficiency factor (E_b) was 3.0×10^{-5} close to 2.0×10^{-5} of the earlier 1-DV simulation of Winterwerp (1998). The empirical erosion constant (M) was estimated to be 1.0×10^{-3} kg/m^2/s, which is slightly larger than the typical value of mud deposits (0.01×10^{-3}~0.5×10^{-3}) (Winterwerp and van Kesteren 2004). The critical shear stress for erosion was set to 1.5 Pa, which is also larger than those of typical mud deposits (0.2~0.8 Pa) (Winterwerp and van Kesteren 2004). Considering the high erosion rate and critical shear stress, cohesive sediments at the measuring site appear to be more resistant to erosion, but they undergo massive erosion once the shear stress exceeds a critical value. The floc characteristic parameters ρ_p and n_f were set to 1,800 kg/m^3 and 2.3, respectively. Remarkably, the fractal dimension corresponds to the maximum of the typical values for mud flocs (1.8~2.3), pointing to the formation of dense and fast-settling flocs at the measuring site. The remaining parameters for hydrodynamics, sediment transport and flocculation kinetics were fixed according to reference values, as shown in Table 3 (Burchard and Baumert 1998; Le Hir et al. 2011; Lee et al. 2011; Winterwerp and van Kesteren 2004). Future research should examine these values more closely.

Simulations of the 1-DV TCPBE were carried out during different tidal cycles using a curve fitted to the measured

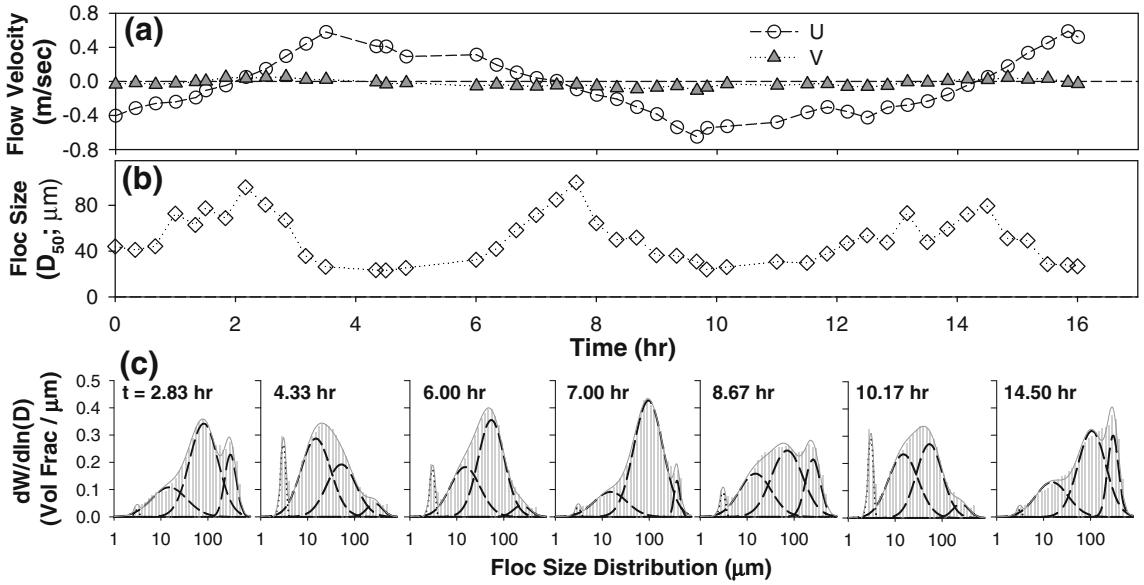

Fig. 3 Time series of **a** the alongshore and cross-shore flow velocities (U, V) at 2 m above the bed (mab) and **b** median floc sizes (D_{50}) at 2 mab, during the time period of Julian day 133.57~114.03. **c** Particle size distributions (PSDs) at different times. The lines inside the envelope of a PSD represent the subordinate PSDs of primary particles, flocculi, microflocs, and macroflocs, from the right to the left of a PSD

friction velocity (U_*) and water height (H) to drive turbulent flow (Fig. 4a). In Fig. 4b, the eddy viscosity represents the flow turbulence and particle/floc resuspension capability in the 1-DV water column. The eddy viscosity of the best-quality simulation was maximal with a bell-shaped profile around the peak flow (e.g., t=4.33 and 10.17 hours). Immediately after slack water, the eddy viscosity reached a minimum and developed a bell-shaped profile skewed towards the bottom (e.g., t=7.00, 8.67 and 14.50 hours). Buoyancy destruction due to the high-rate settling of large flocs and the resulting sediment concentration stratification might explain the form of the profile around slack water. On the other hand, sediment concentration stratification and turbulence destruction were lower than in the other 1-DV simulations (Winterwerp 2011; Winterwerp et al. 2006), probably because erosion and deposition without a fully developed, high concentrated near-bottom mud layer was possible in the bottom boundary of the 1-DV TCPBE.

The simulated profiles of the suspended sediment concentration depend on the fluid turbulence during the tidal cycle (Fig. 4c). For example, the sediment concentration increased during peak flow (e.g., t=4.33 and 10.17 hours), and decreased around slack water (e.g., t=8.67 and 14.50 hours). This suggests that the high turbulence around peak flow enhances erosion and resuspension, thereby bringing sediments upward into the water column. A low turbulence, however, enhances flocculation, settling, and deposition, bringing sediments down to the bottom. The sediment concentration profiles of the best-quality simulation fitted the measured data reasonably, except that they lagged behind the measured data, particularly around slack water (e.g., t=7.00 and 10.17 hours; see also Fig. 5e). This will be discussed later in this section.

The 1-DV TCPBE could simulate the flocculation kinetics during a flow-varying tidal cycle. The simulated profiles of the mean floc size (D_F) were close to the measured data, and increased in size at slack water and decreased during peak flow (Fig. 4d). More importantly, the simulated discrete peaks of flocculi and flocs are an approximation of the measured multimodal PSDs (Fig. 4e). The measured PSDs of flocculi with a high concentration ($N_P \uparrow$) and flocs with a small size and low concentration ($D_F \downarrow$, $N_F \downarrow$) are skewed toward the smaller sizes during peak flow (e.g., t=4.33 and 10.17 hour). During slack water, the measured PSDs are skewed towards a larger size (e.g., t=8.67 and 14.50 hour), which is reflected in the low concentration of flocculi ($N_P \downarrow$) and the high concentration of flocs with a large size ($D_F \uparrow$, $N_F \uparrow$) The results from the 1-DV TCPBE simulation (inverse triangles) followed closely the measured and averaged trajectories of the flocculi and flocs (circles), as shown in Fig. 4e. The 1-DV TCPBE could approximately simulate a multimodal PSD by adjusting the two discrete peaks of the flocculi and flocs, although it could not simulate the entire domain of a multimodal PSD. On the other hand, the 1-DV TCPBE was unable to simulate the floc size growth and sediment accumulation near the bottom, particularly during slack water, because of the open-bottom boundary condition of the 1-DV TCPBE (see Eqs. (11) and (12)) that allows large flocs to settle quickly from the water column. This problem might be solved by combining the model with one that takes near-bottom processes into account.

The best-quality simulation of the 1-DV TCPBE model was reasonably close to the measured data during the entire

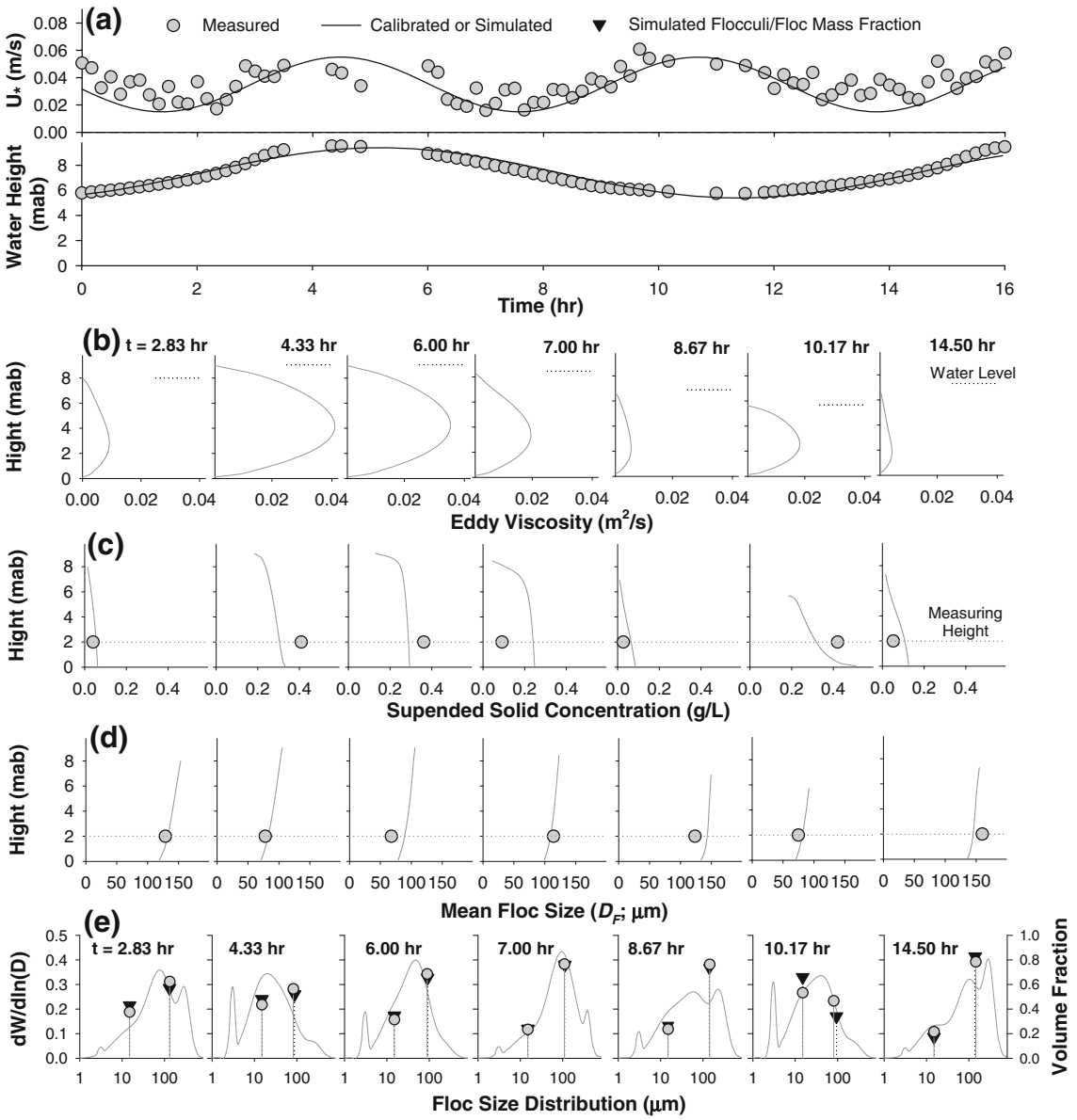

Fig. 4 Time series of **a** measured bottom shear velocities (U_*) and water height (H) and their best-fit tidal equations, during the time period of Julian day 133.57~114.03. **b** Simulated depth profiles of eddy viscosities at different time. Simulated depth profiles and measured data of **c** suspended solid concentrations and **d** volume-mean floc sizes (D_F) at different times. **e** Measured and simulated particle size distributions at different times

measuring period, following the typical up-and-down patterns (Fig. 5). The flocculi mass fraction (f_p) increased to 70 % and the floc size (D_F), which is defined as the mean diameter of flocs, but not of the entire PSD, decreased to 80 μm around peak flow (Fig. 5c, d). This suggests that a high fluid turbulence enhances the breakage of flocs into flocculi and smaller flocs, resulting in the entrainment of flocculi into the water column (see 2.2. Turbulence Closure and Eq. (11)). After peak flow, the flocculi mass fraction (f_p) dropped below 40 % (the floc mass fraction (f_F) increased suddenly to 60 %) but the floc size (D_F) remained small (approximately 80 μm). This behavior suggests that a large number of flocculi, which are entrained from the bed into the water column, aggregated rapidly to small-sized flocs after peak flow, but that the time was insufficient to form large flocs.

Around slack water, the flocculi mass fraction (f_p) decreased to 20 % and the floc size (D_F) increased sharply to 200 μm, indicating that the flocculi aggregated to large flocs during the low fluid turbulence at slack water. The 1-DV TCPBE model could simulate these up-and-down trends of the flocculi mass fraction (f_p) and floc size (D_F) during the entire flood-ebb tidal cycles, but it could not simulate the sharp increase in floc size up to 200 μm around slack water (Fig. 5c). According to Maggi (2009), biologically mediated

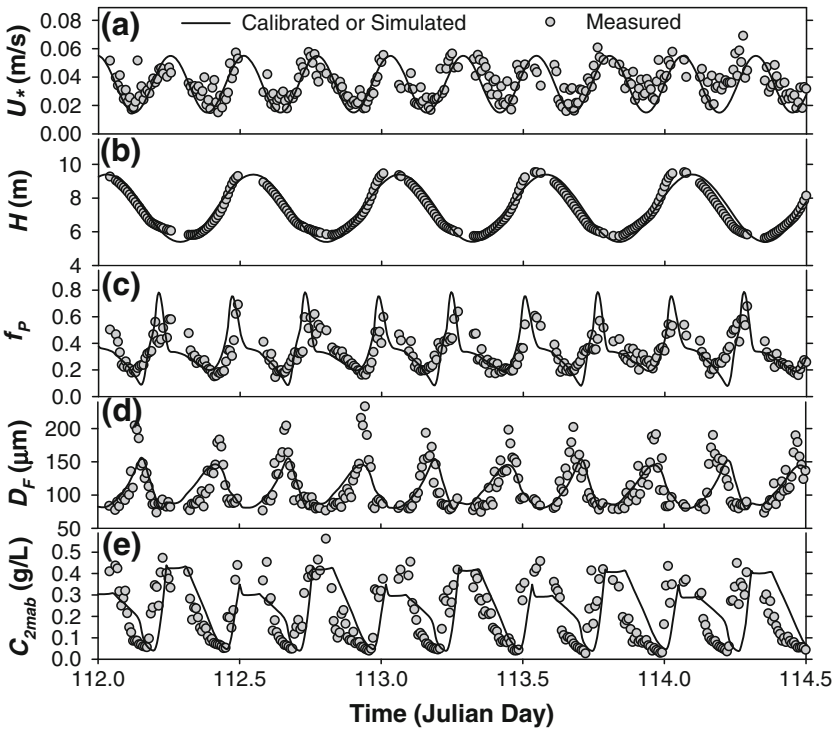

Fig. 5 Time series of the measured and simulated **a** bottom shear velocity (U_*), **b** water height (H), **c** flocculi mass fraction (f_P), **d** volume-mean floc diameter (D_F), and **e** suspended sediment concentration at 2 m above the bed ($C_{2\ mab}$)

flocculation accelerates floc size growth, which can explain the sharp increase in floc size around slack water; biologically mediated flocculation is not incorporated in the 1-DV TCPBE. Another possible explanation for the sharp increase in floc size is the damping of turbulence by the formation of highly concentrated near-bottom sediment suspension layers, which increases the aggregation capability and floc size (Winterwerp 2011). On the other hand, the 1-DV TCPBE model cannot simulate properly the formation of highly concentrated near-bottom suspension layers and the turbulence damping because of the open-bottom boundary for erosion/deposition.

The simulated sediment concentrations are different at high and low water, in contrast to the measured data (see Fig. 5e). As described in Section 2, a change in the water level results in the dilution of cohesive sediments in the water column during high water. Expansion to 2- or 3-D transport models, which take horizontal sediment transport into account, should solve this problem. In addition, it is important to note that the 1-DV TCPBE model resulted in a lag of the simulated sediment concentration behind the measured, particularly around slack water (Fig. 5e; see also Fig. 4c). The measured sediment concentrations decreased and increased faster than the simulated ones, while approaching and leaving the slack water period, respectively. In other words, the measurements showed faster deposition and erosion behavior than the simulations. This possibly points to the occurrence of other processes than the ones incorporated in the 1-DV model (i.e., flocculation, sedimentation, erosion and deposition). Biologically mediated flocculation could be one of the missing processes in the 1-DV TCPBE. Therefore, it is important to know what else is missing in the 1-DV TCPBE model.

The model cannot simulate correctly the formation and disruption of the highly concentrated near-bottom suspension layer and its damping effects on turbulence. Highly concentrated near-bottom suspension layers are formed during low-energy moments around slack water (e.g., Baeye et al. 2011). The measurements, however, were carried out above this expected layer. Therefore, there was no direct evidence for this hypothesis. On the other hand, the present model, like other currently used sediment transport models, has no correlation with the near-bottom boundary conditions in the turbulence model, resulting in an underestimation of turbulence damping, an incorrect bottom shear stress estimation (based on traditional assumptions that ignore drag modulation), and erroneous sediment fluxes in both the horizontal and vertical directions (i.e., transport and erosion, respectively). The model results can only be improved by including these phenomena.

5 Conclusion and recommendations

The results from field measurements and curve-fitting analyses indicated the occurrence of a multimodal PSD consisting of four-level ordered aggregate structures of primary particles, flocculi, microflocs, and macroflocs. The four modal PSDs

could be simplified further into two discrete groups of flocculi and flocs, which led to the idea of developing the TCPBE. The 1-DV TCPBE, combined with the Navier-Stokes equation with the k-ε turbulence closure and sediment mass balance equation, demonstrated its ability to simulate multimodal flocculation and transport of fine-grained cohesive sediments in a marine and coastal environment. In particular, the discrete size groups (i.e., flocculi and flocs) of the 1-DV TCPBE were proven to be a reasonable approximation of a continuous multimodal PSD in modeling and simulation. Because the 1-DV TCPBE model is simple but can simulate multimodal flocculation, it is a promising candidate for modeling flocculation in large-scale multi-dimensional simulations. On the other hand, the 1-DV TCPBE would need to include a high-resolution sediment-fluid interaction model to provide accurate simulations of the formation and disruption of highly concentrated, near-bottom mud suspension layers.

Acknowledgments The authors wish to acknowledge the Flemish Science Foundation (FWO Vlaanderen) for funding the FWO project no. G.0263.08 and the Royal Belgian Institute of Natural Sciences—MUMM for funding the OMFLOC project. This study was funded partly by the Maritime Access Division of the Ministry of the Flemish Community (MOMO project). The mooring and recuperation of the tripod was carried out with the RV Belgica funded by the Belgian Science Policy. The measurements would not have been possible without the technical assistance of L. Naudts and his team (Measuring Service of RBINS-OD Nature, Oostende).

References

Agrawal Y, Pottsmith H (2000) Instruments for particle size and settling velocity observations in sediment transport. Mar Geol 168:89–114

Andrews S, Nover D, Schladow S (2010) Using laser diffraction data to obtain accurate particle size distributions: the role of particle composition. Limnol Oceanogr Methods 8:507–526

Ariathurai, C. (1974), A finite element model for sediment transport in estuaries, PhD Dissertation, University of California, Davis

Aro C, Rodrigue G, Rotman D (1999) A high performance chemical kinetics algorithm for 3-D atmospheric models. Int J High Perform Comput Appl 13(1):3–15

Baeye M, Fettweis M, Voulgaris G, Van Lancker V (2011) Sediment mobility in response to tidal and wind-driven flows along the Belgian inner shelf, southern North Sea. Ocean Dyn 61(5):611–622

Burchard H, Baumert H (1998) The formation of estuarine turbidity maxima due to density effects in the salt wedge. A hydrodynamic process study. J Phys Oceanogr 28:309–321

Burd A, Jackson G (2002) Modeling steady-state particle size spectra. Environ Sci Technol 36:323–327

Conley D, Falchetti S, Lohmann I, Brocchini M (2008) The effects of flow stratification by non-cohesive sediment on transport in high-energy wave-driven flows. J Fluid Mech 610:43–67

Eisma D (1986) Flocculation and de-flocculation of suspended matter in estuaries. Neth J Sea Res 20:183–199

Fettweis M (2008) Uncertainty of excess density and settling velocity of mud flocs derived from in situ measurements. Estuar Coast Shelf Sci 78(2):426–436

Fettweis M, Francken F, Pison V, Van den Eynde D (2006) Suspended particulate matter dynamics and aggregate sizes in a high turbidity area. Mar Geol 235:63–74

Fettweis M, Francken F, Van den Eynde D, Verwaest T, Janssens J, Van Lancker V (2010) Storm influence on SPM concentrations in a coastal turbidity maximum area with high anthropogenic impact (southern North Sea). Cont Shelf Res 30:1417–1427

Fettweis M, Baeye M, Lee B, Chen P, Yu J (2012) Hydro-meteological influences and multimodal suspended particle size distribution in the Belgian nearshore area (southern North Sea). Geo-Mar Lett 32(2): 123–137

Firth B, Hunter R (1976) Flow properties of coagulated colloidal suspensions. J Colloid Interface Sci 57:248–275

Francois R (1985) Studie van de uitvlokking van kaolinietsuspensies met behulp van aluminiumsulfaat. PhD Thesis, University of Leuven, Belgium (in Dutch)

Gibbs R (1985) Estuarine flocs: Their size, settling velocity and density. J Geophys Res 90(c2):3249–3251

Hinds W (1999) Aerosol technology: properties, behavior, and measurement of airborne particles, 2nd edn. Wiley, New York, NY

Huerta A, Liu W (1988) Viscous flow with large free surface motion. Comput Methods Appl Mech Eng 69:277–324

Krone R (1962) Flume studies of the transport of sediment in estuarial shoaling processes. Technical Report, Hydraulic Engineering Laboratory, University of California, Berkeley California, USA

Le Hir P, Cayocca F, Waeles B (2011) Dynamics of sand and mud mixtures: a multiprocess-based modelling strategy. Cont Shelf Res. doi:10.1016/j.csr.2010.12.009

Lee B, Toorman E, Molz F, Wang J (2011) A two-class population balance equation yielding bimodal flocculation of marine or estuarine sediments. Water Res 45(5):2131–2145

Lee B, Fettweis M, Toorman E, Molz F (2012) Multimodality of a particle size distribution of cohesive suspended particulate matters in a coastal zone. J Geophys Res - Ocean 117, C03014. doi:10.1029/2011JC007552

Letter J, Mehta A (2011) A heuristic examination of cohesive sediment bed exchange in turbulent flows. Coast Eng 58(8):779–789

Luyten P, Carniel S, Umgiesser G (2002) Validation of turbulence closure parameterisations for stably stratified flows using the PROVESS turbulence measurements in the North Sea. J Sea Res 47:239–267

Maerz J, Wirtz K (2009) Resolving physically and biologically driven suspended particulate matter dynamics in a tidal basin with a distribution-based model. Estuar Coast Shelf Sci 84: 128–138

Maggi F (2009) Biological flocculation of suspended particles in nutrient-rich aqueous ecosystems. J Hydrol 376:116–125

Manning A, Bass S, Dyer K (2006) Floc properties in the turbidity maximum of a mesotidal estuary during neap and spring tidal conditions. Mar Geol 235:193–211

Michaels A, Bolger J (1962) Settling rates and sediment volumes of flocculated kaoline suspensions. Indian Eng Chem Fund 1:24–33

Munk W, Anderson E (1948) Notes on a theory of the thermocline. J Mar Res 3(1):276–295

Richardson J, Zaki W (1954) Sedimentation and fluidisation, part I. Trans Inst Chem Engrs 2:35–53

Rodi W (1980) Turbulence models and their application in hydraulics, IAHR State-of-the-Art Paper

Schiller L (1932) Fallversuche mit kugeln und scheiben in Handbuch der experimental-Physik, IV., Akademische Verlagsgesellschaft Leipzig

Sherwood C, Lacy J, Voulgaris G (2006) Shear velocity estimates on the inner shelf off Grays Harbor, Washington, USA. Continental Shelf Res 26:1995–2018

Son M, Hsu T (2009) The effect of variable yield strength and variable fractal dimension on flocculation of cohesive sediment. Water Res 43:3582–3592

Toorman E (1999) Sedimentation and self-weight consolidation: constitutive equations and numerical modelling. Geotechnique 49(6):709–726

Toorman E (2003) Validation of macroscopic modelling of particle-laden turbulent flows, in Proceedings 6th Belgian National Congress on Theoretical and Applied Mechanic, Gent

Trowbridge J, Elgar S (2001) Turbulence measurements in the surf zone. J Phys Oceanogr 31:2403–2417

van Leussen W (1994) Estuarine macroflocs: their role in fine-grained sediment transport. Universiteit van Utrecht, The Netherlands

Verney R, Lafite R, Claude Brun-Cottan J, Le Hir P (2011) Behaviour of a floc population during a tidal cycle: laboratory experiments and numerical modelling. Cont Shelf Res 31(10):S64–S83

Weisstein, E. (2006), Log normal distribution, MathWorld—a Wolfram Web Resources. [online] Available from: http://mathworld.wolfram.com/LogNormalDistribution.html (Accessed 22 March 2011).

Whitby K (1978) The physical characteristics of sulfur aerosols. Atmos Environ 41:S25–S49

Winterwerp J (1998) A simple model for turbulence induced flocculation of cohesive sediment. J Hydraul Eng 36(3):309–326

Winterwerp J (2011) Fine sediment transport by tidal asymmetry in the high-concentrated Ems River: indications for a regime shift in response to channel deepening. Ocean Dyn 61(2–3):203–215

Winterwerp J, van Kesteren W (2004) Introduction to the physics of cohesive sediment in the marine environment. Elsevier B.V, Amsterdam, The Netherlands

Winterwerp J, Manning A, Martens C, de Mulder T, Vanlede J (2006) A heuristic formula for turbulence-induced flocculation of cohesive sediment. Estuar Coast Shelf Sci 68:195–207

Xu F, Wang D, Riemer N (2008) Modeling flocculation processes of fine-grained particles using a size-resolved method: comparison with published laboratory experiments. Cont Shelf Res 28:2668–2677